

## Aerodynamics of a wing section along an entry path in Mars atmosphere

Gennaro Zuppardi\*<sup>1</sup> and Giuseppe Mongelluzzo<sup>1,2a</sup>

<sup>1</sup>Department of Industrial Engineering,  
University of Naples "Federico II", Piazzale Tecchio 80, 80125, Naples, Italy

<sup>2</sup>INAF - Astronomical Observatory of Capodimonte, Salita Moiariello 16, 80131, Naples, Italy

(Received August 25, 2020, Revised October 25, 2020, Accepted October 28, 2020)

**Abstract.** The increasing interest in the exploration of Mars stimulated the authors to study aerodynamic problems linked to space vehicles. The aim of this paper is to evaluate the aerodynamic effects of a flapped wing in collaborating with parachutes and retro-rockets to reduce velocity and with thrusters to control the spacecraft attitude. 3-D computations on a preliminary configuration of a blunt-cylinder, provided with flapped fins, quantified the beneficial influence of the fins. The present paper is focused on Aerodynamics of a wing section (NACA-0010) provided with a trailing edge flap. The influence of the flap deflection was evaluated by the increments of aerodynamic force and leading edge pitching moment coefficients with respect to the coefficients in clean configuration. The study was carried out by means of two Direct Simulation Monte Carlo (DSMC) codes (DS2V/3V solving 2-D/3-D flow fields, respectively). A DSMC code is indispensable to simulate complex flow fields on a wing generated by Shock Wave-Shock Wave Interaction (SWSWI) due to the flap deflection. The flap angle has to be a compromise between the aerodynamic effectiveness and the increases of aerodynamic load and heat flux on the wing section lower surface.

**Keywords:** wing section Aerodynamics; hypersonic flow; direct simulation Monte Carlo method; wing-flap deflection; shock wave-shock wave interaction

---

### 1. Introduction

The exploration and the colonization of Mars also involve a careful and deep knowledge of aerodynamic phenomena linked to the interaction between Mars atmosphere and spacecrafts with particular reference to winged vehicles. Indeed, the advantage of a winged spacecraft, compared with that of a non-winged spacecraft, could be in a greater capability to slow down a spacecraft, to control its attitude along the reentry trajectory and finally in a greater precision to land at a predetermined point. Furthermore, the presence of a wing could also reduce the amount of fuel for retro-rockets and thrusters to be loaded on the spacecraft. A possible solution to the design of such a spacecraft, still under study by the authors, is a blunt-cylinder with four fins at 90 deg one from the other, arranged along the axis of the cylinder and provided with flaps. During the descent phase and thanks also to the fins, the cylinder could glide. The gliding phase ends when the blunt-

---

\*Corresponding author, Lecturer, E-mail: [zuppardi@unina.it](mailto:zuppardi@unina.it)

<sup>a</sup>Ph.D. Student, E-mail: [giuseppe.mongelluzzo@unina.it](mailto:giuseppe.mongelluzzo@unina.it)

cylinder will be positioned with vertical axis, making possible the deployment of a parachute and then the ignition of retro-rockets.

The purpose of this paper is to study Aerodynamics of a flapped wing section, representative of the fins, along a Mars entry path. Such a study could be of interest not only for the design of a winged re-entry vehicle but also for future vehicles flying in Mars atmosphere. In fact, the capability of flying in Mars atmosphere could greatly improve the efficiency and the range of both manned and unmanned missions. For this reason, this subject is one of the most relevant topics of the today aerospace research; this problem has already been studied over the last 50 years. Indeed, starting from the Viking I and II missions, a large number of papers have been written on several topics, ranging from theory to experiments, from Computational Fluid Dynamics (CFD) to the Direct Simulation Monte Carlo (DSMC) method (see for example: Reed 1978, French 1986, Anjoi *et al.* 2017, Edquist *et al.* 2014, Huang *et al.* 2016, Golomazov and Finchenko 2014, Raju 2015, Viviani and Pezzella 2013). However, most works are related to Aerodynamics of a classical non-lifting sphere-cone entry capsule. Today, some companies started the design of “conventional” airplanes for flying in Mars atmosphere such as ARES (Aerial Regional-scale Environmental Survey), MAGE (Mars Airborne Geophysical Explorer), AME (Airplane for Mars Exploration), MATADOR (Mars Advanced Technology Airplane for Deployment, Operations and Recovery) (Mars aircraft 2020 and related references), (Guynn *et al.* 2003) and also of drones (Smith *et al.* 2000). Given the extreme conditions of Mars atmosphere produced by very low temperature and density, the development of a well-founded design of a body flying in Mars atmosphere is very challenging. However, due to the very strong interest in this topic, it is possible to foresee in a near future the design of a winged vehicle capable of performing the Entry, Descent, and Landing (EDL) phase on Mars.

To this purpose, an aerodynamic analysis of a wing section provided with a trailing edge flap is important to evaluate the increments of both aerodynamic force and moment as functions of flap deflection. Unfortunately, using a flapped wing section also involves increments of aerodynamic load and heat flux on the wing section lower surface, produced by Shock Wave-Shock Wave Interaction (SWSWI, Bertin 1994). Evaluating the SWSWI effects is necessary for the design of a mechanical and thermal protection system to be installed on the wing surface.

Zuppari (2018a) already studied, computationally, SWSWI in Mars atmosphere. Simulations were carried out considering the NACA-0010 wing section, in the range of angles of attack 0-40 deg, at the altitude of 65 km and with three flap deflections ( $\delta=0, 15, 30$  deg). The free stream or atmosphere parameters were provided by the NASA Glenn model (NASA Glenn Research Center 1996) and velocity was approximated with that of the Pathfinder capsule (Braun and Manning 2006), computed in axi symmetric flow and in free entry, i.e., with no parachutes and no thrusters (Zuppari and Savino 2015). The present work is a logical evolution of the work by Zuppari (2018a). Indeed, computations by Zuppari were carried out at a single altitude (65 km) because the purpose of that work was mainly devoted to study aerodynamic phenomena such as SWSWI, while the purpose of the present work is to evaluate the aerodynamic capability of a flapped surface to cooperate with thrusters and retro-rockets in keeping attitude and in slowing down a spacecraft along an entry path.

Later, specific studies carried out by Zuppari (2018b, 2019a, 2019b, 2020) compared the results computed with the NASA Glenn model with those obtained using the Global Reference Atmospheric Model 2001 (GRAM-2001, Justus and Johnson 2001), again considering velocity from the entry trajectory of Mars Pathfinder. Computations verified that the most significant difference between the NASA Glenn model and the GRAM-2001 is in temperature and

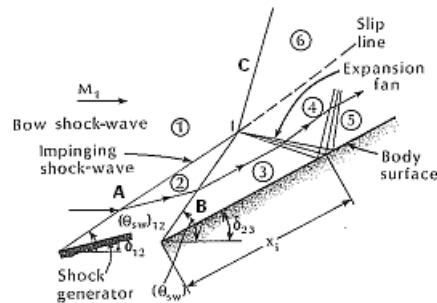


Fig. 1 Sketch of Shock Wave-Shock Wave Interaction (from Bertin 1994)

consequently in density. According to the opinion of the authors, the point of greatest weakness of the Glenn model is in the linear decrease of temperature with altitude ( $h$ ), for  $h > 7000$  m. For example, deep space temperature (4 K) and limit temperature (0 K) would be reached at  $h = 110.6$  km and 112.4 km, respectively.

The effects of the flap deflection both on aerodynamic force and on pitching moment as well as on aerodynamic and thermal loads on the lower surface of the wing section due to SWSWI are quantified. DSMC simulations were carried out on the NACA-0010 wing section in the range of angle of attack ( $\alpha$ ) 0-40 deg and flap deflection ( $\delta$ ) of 0, 15 and 30 deg. Computations were carried out at the altitudes of 60, 80 and 100 km, i.e., before opening of the parachutes and ignition of the retro-rockets. Because of rarefaction, the choice of a specific airfoil is not critical for the present study. The flap angle has to be a compromise between aerodynamic effectiveness and increases of aerodynamic load and heat flux produced by SWSWI on the wing section lower surface. Such increases could also require the installation of a mechanical and thermal protection system on the lower surface of the wing.

The paper consists of a brief 3-D analysis of the finned blunt-cylinder, obtaining useful information about the effects of the presence of fins, playing the role of wings. The analysis then focuses on 2-D Aerodynamics of the flapped wing section. Both global and local quantities are quantified as well as the effects of SWSWI.

## 2. Physics of the shock wave-shock wave interaction

Physics and basic phenomena of the Shock Wave-Shock Wave Interaction (SWSWI) are described by Bertin (1994) and here resumed. In the present paper, SWSWI is produced by the interaction of two oblique shock waves of the same family; a shock wave is produced by the airfoil leading edge, the other one comes from the hinge position of the concave lower surface of the flapped wing section. Fig. 1 provides a scheme of what said; the interacting waves are labeled A and B. Both shock waves are of the same family but with different slopes, thus they can merge at some distance from the surface. The shock wave generated by the interaction is labeled C and the point where the shock waves interact, called "triple point", is labeled as I.

A slip line originates from point I. This slip line separates the flow field in two regions labeled 4 and 6. In region 4, the flow passes through the two shock waves A and B. In the region 6, the flow only passes through the shock wave C. Thus, pressure should be higher in 4 than in 6. In order to decrease pressure in 4 and therefore to restore equilibrium of the slip line, an expansion

fan generates from point I. This fan impinges onto the body surface and reflects again as an expansion fan. Despite the presence of two systems of expansion waves, the shock wave C increases pressure and temperature to values higher than those without SWSWI in the part of the flow field labeled 5, hence on the underlying surface.

### 3. Mars atmosphere, GRAM-2001 and entry trajectory

Mars atmosphere, considered in the present computations, is made of 7 species ( $O_2$ ,  $N_2$ ,  $NO$ ,  $CO$ ,  $CO_2$ ,  $C$ ,  $Ar$ ) and its composition is constant with altitude. Table 1 reports both the mass fraction and the molar fraction of each chemical species. Due to dissociation along an entry path, atomic oxygen and atomic nitrogen are also present. Therefore, for these calculations, Mars atmosphere is a mixture of 9 chemical species. The chemical model proposed by Bird in the version 3.3 of the DS2V code (Bird 2005) and in the version 2.6 of the DS3V code (Bird 2006a) was used. This model is made of 54 reactions: 40 dissociations, 7 forward (or endothermic) exchanges, 7 reverse (or exothermic) exchanges.

The GRAM-2001 is based on the NASA Ames Mars General Circulation Model in the interval 0-80 km and on the Mars Thermosphere General Circulation Model at altitudes above 80 km. Data used in the present paper are those computed by Justus and Johnson (2001). Atmospheric parameters are provided as a function of altitude with a step of about 5 km. Parameters at intermediate altitudes in each step are here computed by linear interpolation. Free stream velocity was approximated with that of the entry trajectory of Pathfinder capsule.

In order to point out the difference between the two models therefore to support the choice of the GRAM-2001, at  $h=100$  km which is of interest for this paper, NASA Glenn model and GRAM-2001 provide temperature of 28 and 127 K, density of  $1.62 \times 10^{-5}$  and  $5.88 \times 10^{-8}$   $kg/m^3$ , respectively. Correspondingly, these differences involve strong variations in the aerodynamic conditions or (by the well known meaning of symbols) in the free stream Mach ( $M_\infty = V_\infty / \sqrt{\gamma RT_\infty}$ ), Reynolds ( $Re_{\infty C} = \rho_\infty V_\infty C / \mu_\infty$ ) and Knudsen ( $Kn_{\infty C} = \lambda_\infty / C$ ) numbers;  $C$  is the wing section chord ( $C=2$  m). At  $h=100$  km,  $M_\infty=84.1$ ,  $Re_C=1.43 \times 10^5$ ,  $Kn_C=8.00 \times 10^{-4}$  are obtained by the Glenn model, while  $M_\infty=39.3$ ,  $Re_C=1.26 \times 10^2$ ,  $Kn_C=4.24 \times 10^{-1}$  are obtained by the GRAM-2001. Since the results from the GRAM-2001 seemed to be more reliable, computations only relied on this model.

Figs. 2(a)-2(d) show the profiles of free stream velocity ( $V_\infty$ ), Mach number ( $M_\infty$ ), Reynolds number ( $Re_{\infty C}$ ), Knudsen number ( $Kn_{\infty C}$ ). In the altitude interval 60-100 km, the flow field around

Table 1 Chemical composition of Mars atmosphere

Chemical species	Mass fraction	Molar fraction
$O_2$	0.0013	0.00176
$N_2$	0.0270	0.04173
$NO$	0.0001	0.00014
$CO$	0.0007	0.00108
$CO_2$	0.9500	0.93399
$C$	0.0049	0.00396
$Ar$	0.0160	0.01734

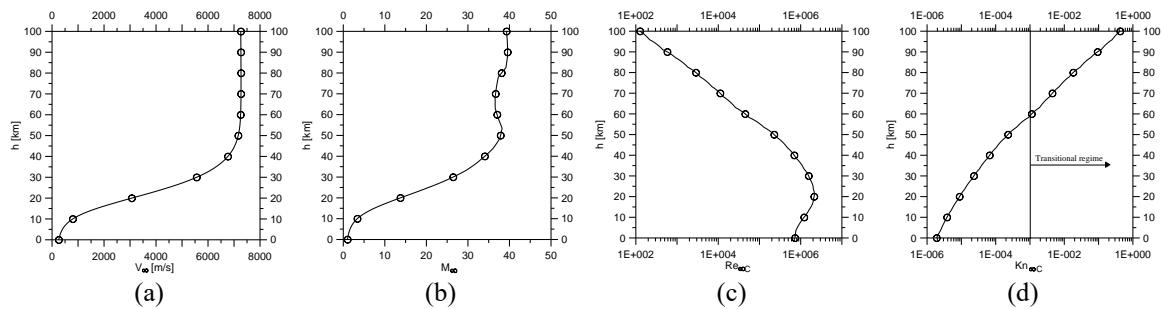


Fig. 2 Profiles of free stream: velocity (a), Mach number (b), Reynolds number (c) and Knudsen number (d) as functions of altitude

the wing section can be reasonably considered in transitional regime. Indeed, according to Moss (1995), the transitional regime is defined in terms of the global Knudsen number by  $10^{-3} < Kn_{\infty C} < 50$ , therefore its solution has to rely on a DSMC code.

#### 4. Direct Simulation Monte Carlo method

It is well known that the Direct Simulation Monte Carlo (DSMC) method (Bird 1998, Bird 2013, Shen 2005) is currently the only available tool for the solution of rarefied flow fields from continuum low density regime (or slip flow) to free molecules regime. DSMC method considers a gas as made up of discrete molecules. It is based on the kinetic theory of gases and computes the evolution of millions of simulated molecules, each one representing a large number of real molecules in the physical space. Molecule-molecule collisions and molecule-surface interactions are computed. The computation domain is divided into cells, used both to select the colliding molecules and to sample the macroscopic, fluid-dynamic quantities. The most important advantage of the method is that it does not suffer from numerical instabilities and does not directly rely on similarity parameters (i.e., Mach, Reynolds and Knudsen numbers). However, it is inherently unsteady. A steady solution is achieved after a sufficiently long simulated time.

The DSMC codes, used in the present study, are the 2-D/axi-symmetric DS2V-4.5 64 bits code (Bird 2008) and DS3V-2.6 (Bird 2006a); these codes are “sophisticated”. As widely reported in literature (Bird 2006b, Bird *et al.* 2009, Gallis *et al.* 2009), a DSMC code is defined sophisticated if it implements computing procedures providing higher efficiency and accuracy with respect to a “basic” DSMC code. A sophisticated code, in fact, considers two sets of cells (collision and sampling) with the related cell adaptation and implements methods promoting “nearest neighbour” collisions. This type of code automatically generates computation parameters such as numbers of cells and of simulated molecules by the input numbers of megabytes and of the free stream number density. It uses a “radial weighting factor” routine in solving axi-symmetric flow fields and provides optimal time steps. Finally, the same collision pair cannot have sequential collisions.

Besides being sophisticated, DS2V-4.5 64 bits and DS3V-2.6 are also advanced; the user can verify that the numbers of simulated molecules and of collision cells are adequate by means of the on line visualization of the ratio between the molecule mean collision separation ( $mcs$ ) and the local mean free path ( $\lambda$ ) in each collision cell. In addition, the codes allow the user to increase, during a computation, the number of simulated molecules. The ratio  $mcs/\lambda$  has to be less than unity everywhere in the computing domain for an acceptable quality of the results. Bird (2006b)

suggests 0.2 as a limit value for an optimal quality of the results. Furthermore, the codes give the user information about the stabilization of a computation by means of the profile of the number of simulated molecules as a function of the simulated time. According to Bird, the stabilization of a DSMC calculation is achieved when this profile becomes jagged and included within a band defining the standard deviation of the number of simulated molecules.

## 5. Test conditions and quality of the computations

Figs. 3(a) and 3(b) show two views of the rendering of the blunt-cylinder with  $\delta=30$  deg. The diameter and the overall length of the blunt-cylinder are  $D=1.6$  m and  $L=4.0$  m. The center of gravity (CG) has been assumed to be located on the axis at  $x_{CG}=1.8$  m. The flapped fins (height 0.3 m) are profiled like a NACA-0010 airfoil, the chord of each flap is 0.4 m. Since the DS3V computations were carried out in symmetric flight, it was possible to consider only half cylinder. RHINOCEROS approximated the blunt-cylinder half-surface into 17380 triangles and the blunt cylinder half-surface with no fins into 9950 triangles. The computation domain was a parallelepiped:  $L_x=5.5$  m,  $L_y=4.0$  m,  $L_z=2.0$  m.

2-D computations were carried out considering a NACA-0010 wing section in clean configuration ( $\delta=0$  deg, Fig. 4(a)) and in flapped configurations:  $\delta=15$  deg (Fig. 4(b)),  $\delta=30$  deg (Fig. 4(c)), already used by Zuppari (2018a). The flap hinge was located at 65% of the chord or at  $x=1.30$  m. The wing section surface was approximated by 1000 flat panels (500 on the lower and 500 on the upper surface). The computation domain was a rectangle:  $L_x=2.5$  m,  $L_y=1.1$  m.

For both 2-D and 3-D computations, the surface was considered non-reactive and reflecting molecules diffusively at a temperature of 300 K, constant along the whole airfoil. Even though this value of surface temperature is not realistic for an entry path, as well known, it is a conventional value to evaluate thermal problems along entry trajectories. Table 2(a) reports input data to DS2V/3V: free stream velocity ( $V_\infty$ ), number density ( $N_\infty$ ), temperature ( $T_\infty$ ). Table 2(b) reports the free stream Mach number ( $Ma_\infty$ ) and also the Reynolds and Knudsen numbers, for the airfoil ( $Re_{\infty C}$ ,  $Kn_{\infty C}$ ) and the blunt-cylinder ( $Re_{\infty L}$ ,  $Kn_{\infty L}$ ).

The quality of the DS2V results can be verified by Table 3(a) where the number of simulated molecules ( $N_M$ ), the ratio of the mean collision separation to the local mean free path ( $mcs/\lambda$ ) and the ratio of simulated time to the fluid-dynamic time ( $t_s/t_f$ ) are reported at each altitude and for

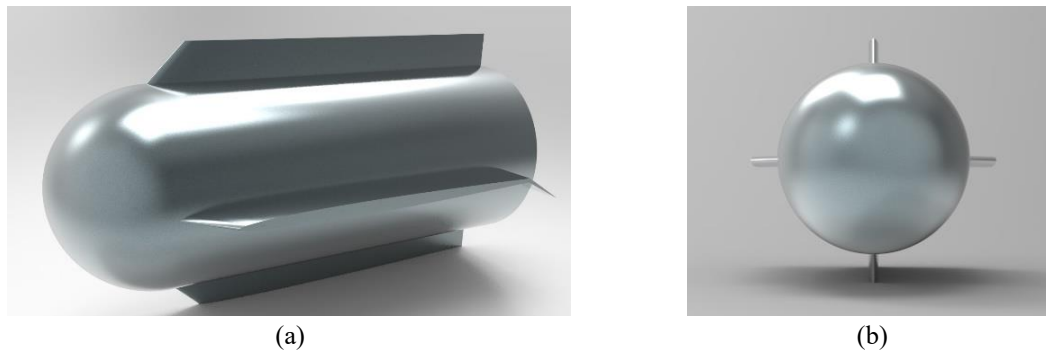


Fig. 3 Rendering of the blunt-cylinder with  $\delta=30$  deg: (a) perspective view, (b) front view

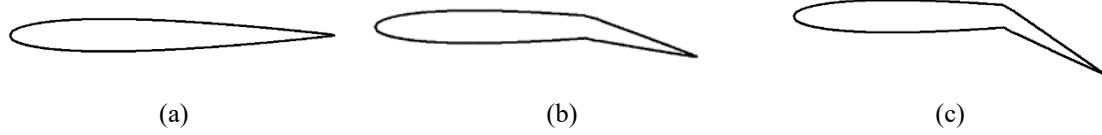
Fig. 4 NACA-0010 wing section with:  $\delta=0$  deg (a),  $\delta=15$  deg (b) and  $\delta=30$  deg (c) (from Zuppardi (2018a))

Table 2(a) DS2V/3V input data

h [km]	$V_\infty$ [m/s]	$N_\infty$ [1/m <sup>3</sup> ]	$T_\infty$ [K]
100	7260	$8.05 \times 10^{17}$	127
90	7265	$3.66 \times 10^{18}$	125
80	7269	$1.94 \times 10^{19}$	135
60	7253	$3.20 \times 10^{20}$	143

Table 2(b) Free stream aerodynamic parameters

h [km]	NACA-0010			Blunt-Cylinder	
	$M_\infty$	$Re_{\infty C}$	$Kn_{\infty C}$	$Re_{\infty L}$	$Kn_{\infty L}$
100	39.3	$1.26 \times 10^2$	$4.24 \times 10^{-1}$	$2.52 \times 10^2$	$2.12 \times 10^{-1}$
90	39.5	$5.80 \times 10^2$	$9.29 \times 10^{-2}$	$1.16 \times 10^3$	$4.64 \times 10^{-2}$
80	38.1	$2.86 \times 10^3$	$1.81 \times 10^{-2}$	$5.72 \times 10^3$	$9.05 \times 10^{-3}$
60	37.0	$4.49 \times 10^4$	$1.12 \times 10^{-3}$	$8.98 \times 10^4$	$5.61 \times 10^{-4}$

Table 3(a) Quality of the DS2V-4.5 64 bits computations

h [km]	$\delta = 0$ deg			$\delta = 15$ deg			$\delta = 30$ deg		
	$N_M$	mcs/ $\lambda$	$t_s/t_f$	$N_M$	mcs/ $\lambda$	$t_s/t_f$	$N_M$	mcs/ $\lambda$	$t_s/t_f$
100	$5.44 \times 10^7$	1.66E-04	5.31	$4.74 \times 10^7$	2.02E-04	4.39	$4.47 \times 10^7$	5.97E-03	3.44
80	$3.84 \times 10^7$	4.78E-03	4.10	$3.45 \times 10^7$	3.67E-03	5.72	$3.70 \times 10^7$	4.67E-03	4.83
60	$3.38 \times 10^7$	6.88E-02	3.11	$3.56 \times 10^7$	7.78E-02	2.66	$3.16 \times 10^7$	8.02E-02	2.30

Table 3(b) Quality of the DS3V-2.6 computations

h [km]	mcs/ $\lambda$	$t_s/t_f$
100	0.05	270
90	0.2	220
80	0.5	160

each flap deflection. The values are averaged over all angles of attack. Table shows that both the DSMC criterion for an optimal quality of results (mcs/ $\lambda < 0.2$ ) and the achievement of a steady condition were satisfied. Indeed, as well known, a rule of thumb suggests that an unsteady fluid-dynamic computation can be considered stabilized when the ratio  $t_s/t_f$  is reasonably greater than unity. Long value of  $t_s$  is beneficial for a DSMC computation because the higher  $t_s$  the higher the number of samples. Thus, the fluctuations could even match those in real gas.

Unfortunately, DS3V outputs only the maximum value of mcs/ $\lambda$  thus the more meaningful

average values reported in Table 3(b) were roughly deduced from a graphic representation of  $mcs/\lambda$  in the meridian plane of the flow field. The values of parameters, reported in Table, are the maximum values of  $mcs/\lambda$  and the minimum values of  $t_s/t_f$  over the whole interval of angles of attack and flap deflections at each altitude. Table verifies that also the DS3V results satisfy the criteria of a good computation.

## 6. Analysis of the results

Figs. 5(a) and 5(b) show, for the blunt-cylinder, the beneficial effects of the fins both on the resultant aerodynamic force ( $F$ ) and on the longitudinal moment, computed considering as reduction pole the center of gravity ( $M_{zCG}$ ) for the case of  $\delta=0$  deg. Fig. 5(b) shows that the blunt-cylinder with and without fins at the three altitudes is in equilibrium at  $\alpha=0$  deg. Thanks to the presence of the fins, the resultant aerodynamic force increases at each altitude from about 9% to 22% in the interval of angles of attack 0-40 deg. Much more than this, the fins increase the magnitude of the stability derivative ( $(dM_{zCG}/d\alpha)_{\alpha_{eq}}$ ). As well known, equilibrium is stable if derivative is negative, unstable if derivative is positive and the magnitude of derivative is a measure of equilibrium. For example, at the intermediate altitude of 90 km stability increases; the magnitude of the stability derivative increases from  $|-0.047|$  to  $|-0.177|$  while, at  $h=80$  km, instability decreases. In fact, the stability derivative reduces from 0.724 to 0.188. These preliminary 3-D results verify that the effect of the fins is meaningful therefore stimulated the authors to deepen the aerodynamic study of a wing section in Mars atmosphere.

Figs. 6(a)-6(d) show the profiles of the lift ( $C_l$ ), drag ( $C_d$ ), aerodynamic force ( $C_F$ ), leading edge pitching moment ( $C_{mLE}$ ) coefficients with the three flap deflections at the intermediate altitude of  $h=80$  km for the NACA-0010 airfoil. The effects of flap deflection are quantified by the increments of the resultant aerodynamic force ( $\Delta C_F$ ) and of the leading edge pitching moment ( $\Delta C_{mLE}$ ) coefficients with respect to the same quantities in clean configuration.  $\Delta C_F$  and  $\Delta C_{mLE}$  are measures of the capability to reduce the velocity of spacecraft and to control its attitude along an entry path, respectively.

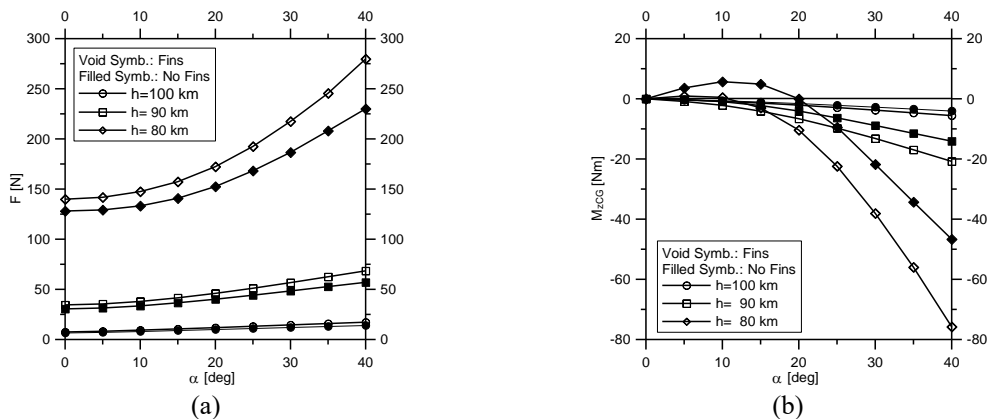


Fig. 5 Profiles of the resultant aerodynamic force (a) and of longitudinal moment (b) as functions of the angle of attack:  $\delta=0$  deg

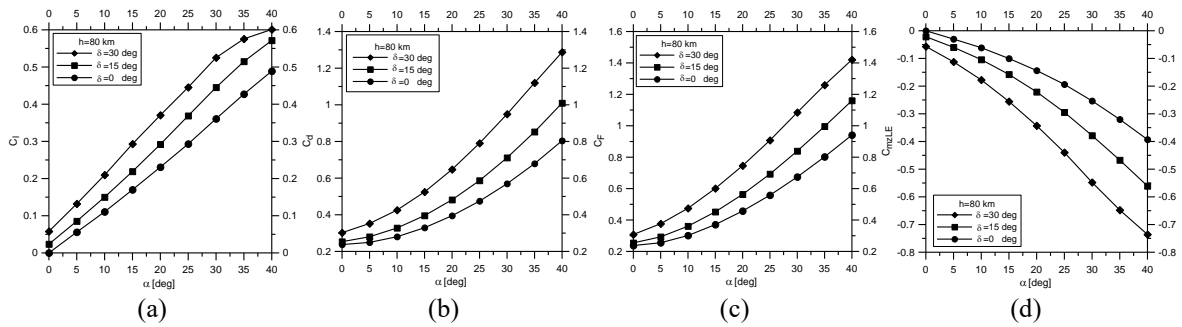


Fig. 6 Profiles of lift (a), drag (b), aerodynamic force (c) and leading edge pitching moment (d) coefficients for the NACA-0010 wing section:  $h=80$  km

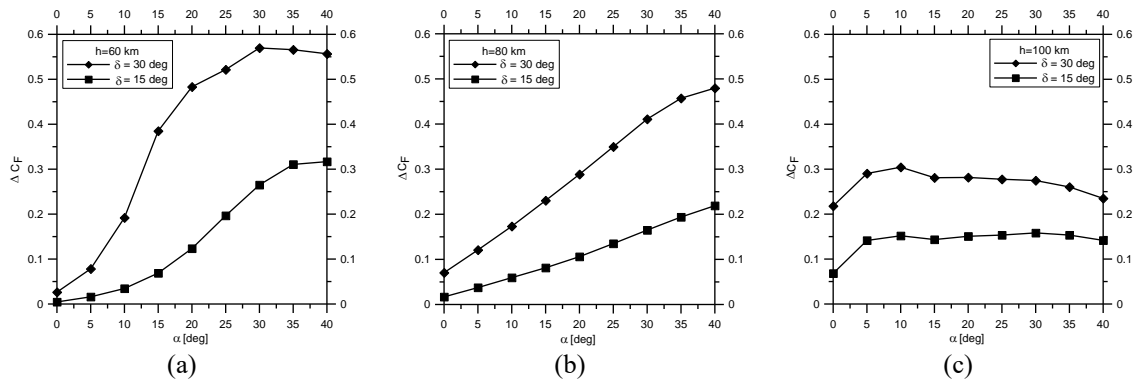


Fig. 7 Profiles of the increment of the resultant aerodynamic force coefficient for the NACA-0010 wing section:  $h=60$  (a), 80 (b) and 100 (c) km

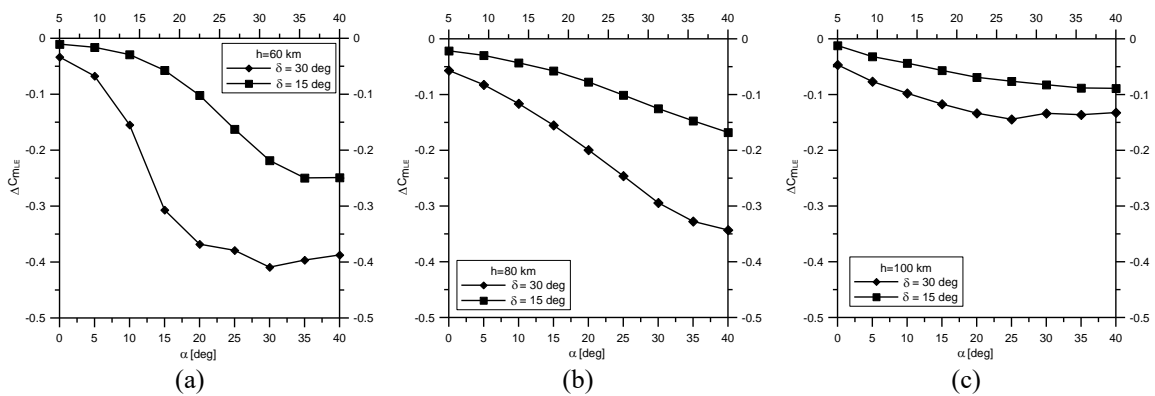


Fig. 8 Profiles of the increment of the leading edge pitching moment coefficient for the NACA-0010 wing section:  $h=60$  (a), 80 (b) and 100 (c) km

Figs.7(a)-7(c) and 8(a)-8(c) show the profiles of  $\Delta C_F$  and  $\Delta C_{mLE}$  as functions of the angle of attack computed at the three altitudes with  $\delta=15$  and 30 deg, respectively. Tables 4(a) and 4(b) report the values of  $\Delta C_F$  and  $\Delta C_{mLE}$  for each angle of attack, the three altitudes and the two flap deflections. Figures and tables show that, at the altitudes of  $h=60$  and 80 km, the effect of the flap

Table 4(a) Increments of the resultant aerodynamic force and leading edge pitching moment coefficient for the NACA-0010 wing section:  $\delta=15$  deg

$\alpha$ [deg]	h=60 km		h=80 km		h=100 km	
	$\Delta C_F$	$\Delta C_{MLE}$	$\Delta C_F$	$\Delta C_{MLE}$	$\Delta C_F$	$\Delta C_{MLE}$
0	0.0046	-0.0104	0.0169	-0.0215	0.0681	-0.0121
5	0.0160	-0.0161	0.0375	-0.0297	0.1414	-0.0318
10	0.0345	-0.0291	0.0595	-0.0430	0.1518	-0.0436
15	0.0688	-0.0572	0.0814	-0.0574	0.1434	-0.0567
20	0.1235	-0.1018	0.1060	-0.0773	0.1507	-0.0690
25	0.1966	-0.1624	0.1350	-0.1009	0.1534	-0.0761
30	0.2650	-0.2184	0.1649	-0.1252	0.1582	-0.0823
35	0.3106	-0.2496	0.1938	-0.1471	0.1534	-0.0882
40	0.3168	-0.2490	0.2190	-0.1679	0.1416	-0.0888

Table 4(b) Increments of the resultant aerodynamic force and leading edge pitching moment coefficient for the NACA-0010 wing section:  $\delta=30$  deg

$\alpha$ [deg]	h=60 km		h=80 km		h=100 km	
	$\Delta C_F$	$\Delta C_{MLE}$	$\Delta C_F$	$\Delta C_{MLE}$	$\Delta C_F$	$\Delta C_{MLE}$
0	0.0264	-0.0334	0.0705	-0.0567	0.2180	-0.0466
5	0.0783	-0.0674	0.1209	-0.0823	0.2904	-0.0766
10	0.1920	-0.1547	0.1733	-0.1162	0.3044	-0.0977
15	0.3849	-0.3069	0.2304	-0.1550	0.2810	-0.1171
20	0.4832	-0.3681	0.2885	-0.1993	0.2816	-0.1334
25	0.5215	-0.3791	0.3496	-0.2460	0.2776	-0.1443
30	0.5697	-0.4092	0.4109	-0.2942	0.2747	-0.1337
35	0.5658	-0.3965	0.4571	-0.3275	0.2604	-0.1362
40	0.5567	-0.3873	0.4796	-0.3430	0.2350	-0.1323

deflection increases with the angle of attack and that, because of rarefaction, at the altitude of  $h=100$  km its dependence on the angle of attack reduces. It seems that at  $h=100$  km and for both flap angles, the greatest  $\Delta C_F$  is achieved at  $\alpha \approx 10$  deg.

Unfortunately, the beneficial effects produced by the flap deflection are counterbalanced by the effects of SWSWI which, as already said, produces increments of pressure and heat flux on the flap lower surface in hyper/supersonic flows. The SWSWI effects in the flow field or the increments of temperature and pressure can be visualized in Figs. 9(a)-9(c) and Figs. 10(a)-10(c) where 2-D maps of temperature and pressure, for example at  $h=80$  km and at the most severe condition of  $\alpha=40$  deg, are shown for  $\delta=0$  (a),  $\delta=15$  (b) and  $\delta=30$  (c) deg. These increments produce, in turn, increases of heat flux and pressure or aerodynamic load on the flap lower surface, respectively.

Figs. 11(a)-11(c) and 12(a)-12(c) show the profiles of pressure and heat flux along the wing section lower surface at  $\alpha=40$  deg. As shown in Figs. 11(a) and 12(a), pressure and heat flux at  $h=60$  km are even higher than those on the leading edge. The sudden decreases in the profiles of

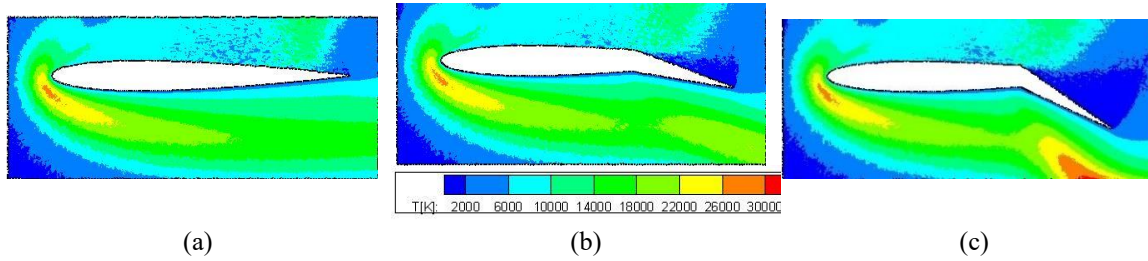


Fig. 9 2-D maps of temperature in the flow field around the NACA-0010 wing section for the three flap deflections:  $h=80$  km,  $\alpha=40$  deg

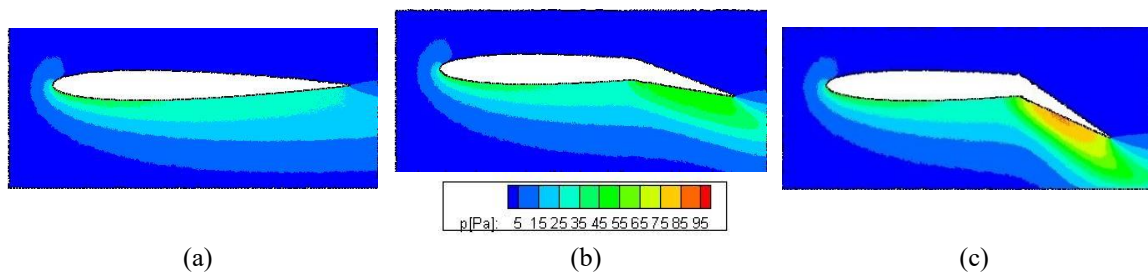


Fig. 10 2-D maps of pressure in the flow field around the NACA-0010 wing section for the three flap deflections:  $h=80$  km,  $\alpha=40$  deg

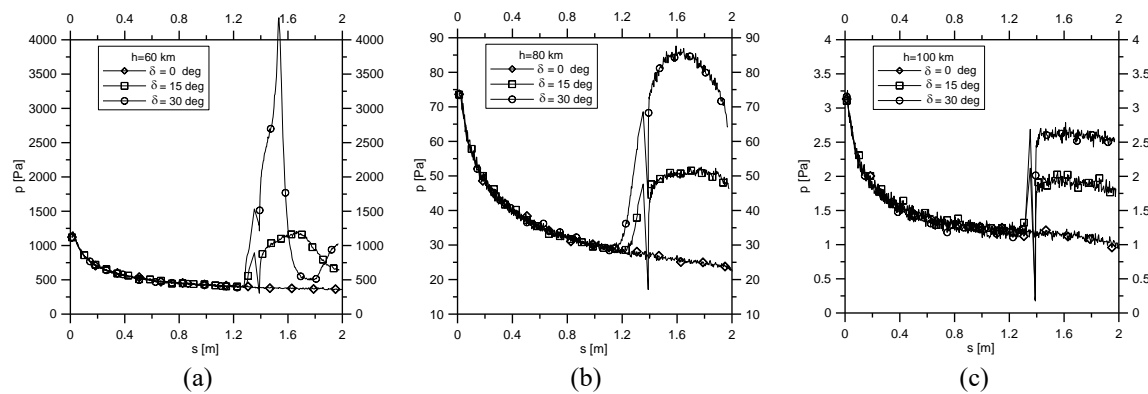


Fig. 11 Profiles of pressure distribution on the lower surface of the NACA-0010 wing section for the three flap deflections at the three altitudes:  $h=60$  (a),  $80$  (b) and  $100$  (c) km

both pressure and heat flux at  $s \cong 1.40$  m (or  $x \cong 1.30$  m, i.e., close to the flap hinge position), are probably due to a local, small flow separation.

In analogy with what done for the force and the moment coefficients, the effects of SWSWI on the flap lower surface are quantified by the differences between the maximum and minimum pressure and heat flux on the flap lower surface:  $\Delta p_{\max} = p_{\max} - p_{\min}$ ,  $\Delta \dot{q}_{\max} = \dot{q}_{\max} - \dot{q}_{\min}$ . The minimum values of these quantities are related to clean configuration. Figs.13(a) and 13(b) show the profiles of  $\Delta p_{\max}$  and  $\Delta \dot{q}_{\max}$  as functions of the angle of attack at the intermediate altitude of 80 km. Figures show that the maximum effects of SWSWI for pressure and heat flux do not happen at the same angle of attack.

Table 5(a) Increments of pressure and heat flux on the flap lower surface of the NACA-0010 wing section:  $\delta=15$  deg

$\alpha$ [deg]	h=60 km		h=80 km		h=100 km	
	$\Delta p_{\max}$ [Pa]	$\Delta \dot{q}_{\max}$ [W/m <sup>2</sup> ]	$\Delta p_{\max}$ [Pa]	$\Delta \dot{q}_{\max}$ [W/m <sup>2</sup> ]	$\Delta p_{\max}$ [Pa]	$\Delta \dot{q}_{\max}$ [W/m <sup>2</sup> ]
0	23	31	3.39	10.43	0.13	1.14
5	46	45	5.50	13.66	0.28	2.76
10	91	68	8.38	17.10	0.42	3.13
15	185	87	10.98	19.17	0.54	2.80
20	341	129	14.74	22.75	0.69	3.01
25	520	171	19.46	24.57	0.80	3.12
30	623	162	24.74	26.52	0.92	3.21
35	758	199	27.88	25.57	1.04	3.21
40	864	229	30.27	22.93	1.12	3.19

Table 5(b) Increments of pressure and heat flux on the flap lower surface of the NACA-0010 wing section:  $\delta=30$  deg

$\alpha$ [deg]	h=60 km		h=80 km		h=100 km	
	$\Delta p_{\max}$ [Pa]	$\Delta \dot{q}_{\max}$ [W/m <sup>2</sup> ]	$\Delta p_{\max}$ [Pa]	$\Delta \dot{q}_{\max}$ [W/m <sup>2</sup> ]	$\Delta p_{\max}$ [Pa]	$\Delta \dot{q}_{\max}$ [W/m <sup>2</sup> ]
0	114	88	12.08	31.03	0.68	4.38
5	283	159	17.76	35.73	0.91	5.22
10	747	295	24.64	40.55	1.14	5.58
15	1311	382	32.05	44.39	1.29	5.12
20	1689	476	40.35	47.81	1.48	5.10
25	1936	565	48.54	50.08	1.64	5.21
30	2191	515	56.76	44.18	1.71	5.51
35	2865	851	62.22	40.03	1.77	5.34
40	3979	1360	65.28	35.52	1.85	5.23

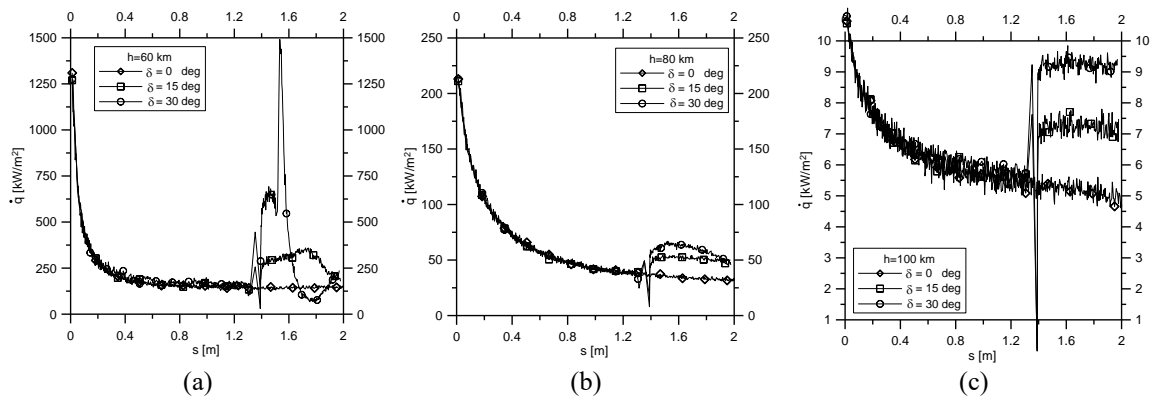


Fig. 12 Profiles of heat flux distribution on the lower surface of the NACA-0010 wing section for the three flap deflections and at the three altitudes: h=60 (a), 80 (b) and 100 (c) km

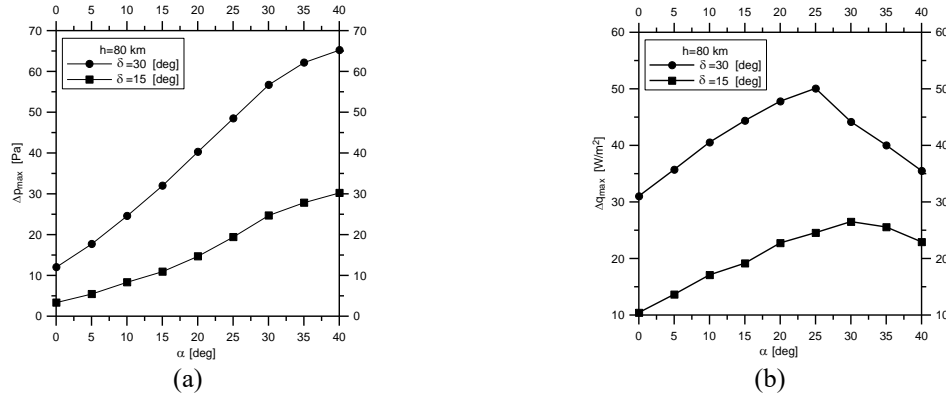


Fig. 13 Profiles of the increments of pressure (a) and heat flux (b) on the lower surface of the NACA-0010 wing section for two flap deflections:  $h=80$  km

Tables 5(a) and 5(b) report the values of  $\Delta p_{\max}$  and  $\Delta \dot{q}_{\max}$  at each angle of attack and with  $\delta=15$  and 30 deg, respectively. As expected,  $\Delta p_{\max}$  and  $\Delta \dot{q}_{\max}$  get the highest values at the most severe test conditions of  $h=60$  km,  $\delta=30$  deg and  $\alpha=40$  deg. Both  $\Delta p_{\max}$  and  $\Delta \dot{q}_{\max}$  increase of an order of magnitude in the interval 0-40 deg. More specifically, pressure and heat flux increase of one and two orders of magnitude for  $\delta=15$  and 30 deg, respectively. The variability of  $\Delta p_{\max}$  and  $\Delta \dot{q}_{\max}$  with the angle of attack decreases with altitude or with rarefaction. The optimal flap deflection has to be a compromise between the effectiveness of the flap deflection and the increments of aerodynamic load and heat flux, demanding for the installation of a mechanical and thermal protection system on the flap lower surface.

## 7. Conclusions

The exploration and the forthcoming colonization of Mars stimulated the study of aerodynamic problems concerning the use of aerodynamic surfaces provided with flaps. The aim of the paper was to evaluate the increases of both the resultant aerodynamic force and the pitching moment linked to the flap deflection at high altitude along an entry path. Flapped surfaces can cooperate with parachutes and retro-rockets for the reduction of the spacecraft velocity along an entry path and mainly with thrusters for the control of its attitude. To this purpose, the use of flapped surfaces is interesting because it could involve a reduction of propellant to be loaded on the spacecraft.

Computations, carried out on a preliminary configuration of a blunt-cylinder, provided of four flapped fins arranged along the cylinder axis at 90 deg one from the other, verified the beneficial influence of the fins and stimulated investigation about Aerodynamics of wings flying in Mars atmosphere; computations were carried out on a NACA-0010 wing section. 2-D computations were carried out at altitudes of 60, 80 and 100 km, 3-D computations at altitudes of 80, 90 and 100 km, both in the range of attack angle 0-40 deg and using atmosphere parameters from the GRAM-2001. The 3-D computations were performed with no flap deflection, those 2-D with flap deflections of 0, 15 and 30 deg. The computations were carried out by means of two Direct Simulation Monte Carlo codes: DS3V-2.6 for the 3-D, DS2V-4.5 64 bits for the 2-D computations.

The increases of both resultant aerodynamic force and pitching moment as well as the SWSWI

effects were quantified. The flap deflection has to be a compromise between the effectiveness of the flap and the increases of both aerodynamic load and heat flux on the lower surface of the flap which should be provided with a mechanical and thermal protection system.

The results obtained in the present work encourage the development of a winged spacecraft with flapped surfaces to help the spacecraft, entering Mars atmosphere, to reduce velocity and to keep attitude. These spacecrafts will be alternative to the “classical”, non-lifting sphere-cone capsule.

## Acknowledgments

This research did not receive any specific grant from funding agencies in the public, commercial, or not-for-profit sectors.

## References

- Anyoji, M., Okamoto, M., Fujita, K., Nagai, H. and Oyama, A. (2017), “Evaluation of aerodynamic performance of Mars airplane in scientific balloon experiment”, *Fluid Mech. Res. Int.*, **1**(3), 1-7. <https://doi.org/10.15406/fmrij.2017.01.00012>.
- Bertin, J.J. (1994), *Hypersonic Aerothermodynamics*, AIAA Education Series, Washington, D.C., U.S.A.
- Bird, G.A. (1998), *Molecular Gas Dynamics and Direct Simulation Monte Carlo*, Clarendon Press, Oxford, U.K.
- Bird, G.A. (2005), *The DS2V Program User's Guide Ver. 3.3*, G.A.B. Consulting Pty Ltd, Sydney, Australia.
- Bird, G.A. (2006a), *Visual DSMC Program for Three-Dimensional Flows, the DS3V Program User's Guide, Ver. 2.6*, G.A.B. Consulting Pty Ltd, Sydney, Australia.
- Bird, G.A. (2006b), “Sophisticated versus simple DSMC”, *Proceedings of the 25th International Symposium on Rarefied Gas Dynamics (RGD25)*, Saint Petersburg, Russia, July.
- Bird, G.A. (2008), *Visual DSMC Program for Two-Dimensional Flows, the DS2V Program User's Guide, Ver. 4.5*, G.A.B. Consulting Pty Ltd, Sydney, Australia.
- Bird, G.A. (2013), *The DSMC Method, Version 1.1*, CreateSpace Independent Publ. Platform, Charleston, South Carolina, U.S.A.
- Bird, G.A., Gallis, M.A., Torczynski, J.R. and Rader, D.J. (2009), “Accuracy and efficiency of the sophisticated Direct Simulation Monte Carlo algorithm for simulating non-continuum gas flows”, *Phys. Fluids*, **21**(1), 1-12. <https://doi.org/10.1063/1.3067865>.
- Braun, R.D. and Manning, R.M. (2006), “Mars exploration entry, descent and landing challenges”, *Proceedings of the 2006 IEEE Aerospace Conference*, Big Sky, Minnesota, U.S.A., March.
- Edquist, K.T., Hollis, B.R., Johnston, C.O., Bose, D., White, T.R. and Mahzari, M. (2014), “Mars science laboratory heatshield aerothermodynamics: Design and reconstruction”, *J. Spacecraft Rockets*, **51**(4), 1106-1124. <https://doi.org/10.2514/1.A32749>.
- French, J.R. (1986), “The Mars airplane”, NASA Marshall Space Flight Center Manned Mars Missions, Working Group Papers, 1, Section 1-4, 406-414.
- Gallis, M.A., Torczynski, J.R., Rader, D.J. and Bird, G.A. (2009), “Convergence behavior of a new DSMC algorithm”, *J. Comput. Phys.*, **228**(12), 4532-4548. <https://doi.org/10.1016/j.jcp.2009.03.021>.
- Golomazov, M.M. and Finchenko, V.S. (2014), “Aerodynamic design of a descent vehicle in Martian atmosphere under ExoMars project”, *Solar Syst. Res.*, **48**(7), 541-548. <https://doi.org/10.1134/S0038094614070089>.
- Guynn, M.D., Croom, M.A., Smith, S.C., Parks, R.W. and Gelhausen, P.A. (2003), “Evolution of a Mars airplane concept for the ARES Mars scout mission”, *Proceedings of the 2nd AIAA “Unmanned*

- Unlimited” *Systems, Technologies, and Operations – Aerospace*, San Diego, California, U.S.A., September.
- Huang, F., Jin, X.G., Lv, J.M. and Cheng, X.L. (2016), “Impact of Martian parameter uncertainties on entry vehicles Aerodynamics for hypersonic rarefied conditions”, *Proceedings of the 30th International Symposium on Rarefied Gas Dynamics:RGD 30*, Victoria, British Columbia, Canada, July.
- Justus, C.G. and Johnson, D.L. (2001), *Mars Global Reference Atmospheric Model 2001 (Mars-GRAM-2001) User Guide*, NASA TM 2001-210961, NASA.
- Mars Aircraft (2020), [https://en.wikipedia.org/wiki/Mars\\_aircraft#Airplanes](https://en.wikipedia.org/wiki/Mars_aircraft#Airplanes).
- Moss, J.N. (1995), “Rarefied flows of planetary entry capsules”, AGARD-R-808, 95-129, *Proceedings of the Special Course on “Capsule Aerothermodynamics”*, Rhode-Saint-Genèse, Belgium, May.
- NASA Glenn Research Center, Mars Atmosphere Model (1996), <https://www.grc.nasa.gov/WWW/K-12/airplane/atmosmre.html>.
- Raju, M. (2015), “CFD analysis of Mars Phoenix capsules at Mach number 10”, *J. Aeronaut. Aero. Eng.*, **4**(1), 1-4. <https://doi.org/10.4172/2168-9792.1000141>.
- Reed, R.D. (1978), “High-flying Mini-Sniffer RPV - Mars bound”, *Astronaut. Aeronaut.*, **16**, 26-39.
- Shen, C. (2005), *Rarefied Gas Dynamic: Fundamentals, Simulations and Micro Flows*, Springer-Verlag, Berlin, Germany.
- Smith, S.C., Hahn, A.S., Johnson, W.R., Kinnery, D.J., Pollitt, J.A. and Reuther, J.J. (2000), “The design of the Canyon Flyer, an airplane for Mars exploration”, *Proceedings of the 38th Aerospace Sciences Meeting and Exhibit*, Reno, Nevada, U.S.A., January.
- Viviani, A. and Pezzella, G. (2013), “Non-equilibrium computational flow field analysis for the design of Mars manned entry vehicles”, *Prog. Flight Phys.*, **5**, 493-516. <https://doi.org/10.1051/eucass/201305493>.
- Zuppari, G. (2018a), “Effects of SWBLI and SWSWI in Mars atmosphere entry”, *Proceedings of the 31st International Symposium on Rarefied Gas Dynamics (RGD31)*, Glasgow, U.K., July.
- Zuppari, G. (2018b), “Effects of chemistry in Mars entry and Earth re-entry”, *Adv. Aircraft Spacecraft Sci.*, **5**(1), 581-594. <https://doi.org/10.12989/aas.2018.5.5.581>.
- Zuppari, G. (2019a), “Influence of the Mars atmosphere model on aerodynamics of an entry capsule”, *Adv. Aircraft Spacecraft Sci.*, **6**(3), 239-256. <https://doi.org/10.12989/aas.2019.6.3.239>.
- Zuppari, G. (2019b), “Influence of the Mars Atmosphere Model on 3-D aerodynamics of an entry capsule”, *Proceedings of the Direct Simulation Monte Carlo Workshop DSMC19*, Santa Fe, New Mexico, U.S.A., September.
- Zuppari, G. (2020), “Influence of the Mars atmosphere model on aerodynamics of an entry capsule: Part II”, *Adv. Aircraft Spacecraft Sci.*, **7**(3), 229-249. <https://doi.org/10.12989/aas.2020.7.3.229>.
- Zuppari, G. and Savino, R. (2015), “DSMC Aero-thermo-dynamic analysis of a deployable capsule for Mars atmosphere entry”, *Proceedings of the Direct Simulation Monte Carlo Workshop DSMC15*, Kauai, Hawaii, U.S.A., September.